Wang, Jinzhang; Cai, Zhiping; Xu, Ping; Du, Geguo; Wang, Fengqiu; Ruan, Shuangchen; Sun, Zhipei; Hasan, Tawfique

Pulse dynamics in carbon nanotube mode-locked fiber lasers near zero cavity dispersion

Published in:
Optics Express

DOI:
10.1364/OE.23.009947

Published: 01/01/2015

Document Version
Publisher's PDF, also known as Version of record

Pulse dynamics in carbon nanotube mode-locked fiber lasers near zero cavity dispersion

Jinzhang Wang,[1] Zhiping Cai,[2] Ping Xu,[3] Geguo Du,[3] Fengqiu Wang,[4] Shuangchen Ruan,[1,*] Zhipei Sun,[5] and Tawfique Hasan[6]

[1]*College of Optoelectronic Engineering, Shenzhen University, Shenzhen 518060, China*
[2]*Department of Electronics Engineering, Xiamen University, Xiamen 361005, China*
[3]*School of Electronic Science and Technology, Shenzhen University, Shenzhen 518060, China*
[4]*School of Electronic Science and Engineering and Collaborative Innovation Center of Advanced Microstructures, Nanjing University, Nanjing 210093, China*
[5]*Department of Micro- and Nanosciences, Aalto University, Aalto, FI-00076, Finland*
[6]*Cambridge Graphene Centre, University of Cambridge, Cambridge CB3 0FA, UK*
[*]*scruan@szu.edu.cn*

Abstract: We numerically and experimentally analyze the output characteristics and pulse dynamics of carbon nanotube mode-locked fiber lasers near zero cavity dispersion (from 0.02 to ~–0.02 ps^2). We focus on such near zero dispersion cavities to reveal the dispersion related transition between different mode-locking regimes (such as soliton-like, stretched-pulse and self-similar regimes). Using our proposed model, we develop a nanotube-mode-locked fiber laser setup generating ~97 fs pulse which operates in the stretched-pulse regime. The corresponding experimental results and pulse dynamics are in good agreement with the numerical results. Also, the experimental results from soliton-like and self-similar regimes exhibit the same trends with simulations. Our study will aid design of different mode-locking regimes based on other new saturable absorber materials to achieve ultra-short pulse duration.

OCIS codes: (140.4050) Mode-locked lasers; (140.7090) Ultrafast lasers; (160.4236) Nanomaterials.

References and links

1. Y.-C. Cheng and G. R. Fleming, "Dynamics of light harvesting in photosynthesis," Annu. Rev. Phys. Chem. **60**(1), 241–262 (2009).
2. J. M. Dudley, G. Genty, and S. Coen, "Supercontinuum generation in photonic crystal fiber," Rev. Mod. Phys. **78**(4), 1135–1184 (2006).
3. T. Udem, R. Holzwarth, and T. W. Hänsch, "Optical frequency metrology," Nature **416**(6877), 233–237 (2002).
4. U. Keller, "Recent developments in compact ultrafast lasers," Nature **424**(6950), 831–838 (2003).
5. M. E. Fermann and I. Hartl, "Ultrafast fiber laser technology," IEEE J. Sel. Top. Quantum Electron. **15**(1), 191–206 (2009).
6. F. W. Wise, A. Chong, and W. H. Renninger, "High-energy femtosecond fiber lasers based on pulse propagation at normal dispersion," Laser Photon. Rev. **2**(1-2), 58–73 (2008).
7. L. E. Nelson, D. J. Jones, K. Tamura, H. A. Haus, and E. P. Ippen, "Ultrashort-pulse fiber ring lasers," Appl. Phys. B **65**(2), 277–294 (1997).
8. A. Chong, W. H. Renninger, and F. W. Wise, "Properties of normal-dispersion femtosecond fiber lasers," J. Opt. Soc. Am. B **25**(2), 140–148 (2008).
9. H. A. Haus, J. G. Fujimoto, and E. P. Ippen, "Structures for additive pulse mode locking," J. Opt. Soc. Am. B **8**(10), 2068–2076 (1991).
10. K. Tamura, E. P. Ippen, H. A. Haus, and L. E. Nelson, "77-fs pulse generation from a stretched-pulse mode-locked all-fiber ring laser," Opt. Lett. **18**(13), 1080–1082 (1993).
11. K. Tamura, E. P. Ippen, and H. A. Haus, "Pulse dynamics in stretched-pulse fiber lasers," Appl. Phys. Lett. **67**(2), 158–160 (1995).
12. H. A. Haus, K. Tamura, L. E. Nelson, and E. P. Ippen, "Stretched-pulse additive pulse mode-locking in fiber ring lasers: theory and experiment," IEEE J. Quantum Electron. **31**(3), 591–598 (1995).
13. R. Herda and O. G. Okhotnikov, "Dispersion compensation-free fiber laser mode-locked and stabilized by high-contrast saturable absorber mirror," IEEE J. Quantum Electron. **40**(7), 893–899 (2004).

#231628 - $15.00 USD Received 30 Dec 2014; revised 31 Mar 2015; accepted 3 Apr 2015; published 10 Apr 2015

14. M. Guina, N. Xiang, A. Vainionpää, O. G. Okhotnikov, T. Sajavaara, and J. Keinonen, "Self-starting stretched-pulse fiber laser mode locked and stabilized with slow and fast semiconductor saturable absorbers," Opt. Lett. **26**(22), 1809–1811 (2001).
15. F. X. Kurtner, J. A. der Au, and U. Keller, "Mode-locking with slow and fast saturable absorbers-what's the difference?" IEEE J. Sel. Top. Quantum Electron. **4**(2), 159–168 (1998).
16. R. Herda and O. G. Okhotnikov, "Effect of amplified spontaneous emission and absorber mirror recovery time on the dynamics of mode-locked fiber lasers," Appl. Phys. Lett. **86**(1), 011113 (2005).
17. U. Keller, K. J. Weingarten, F. X. Kartner, D. Kopf, B. Braun, I. D. Jung, R. Fluck, C. Honninger, N. Matuschek, and J. Aus der Au, "Semiconductor saturable absorber mirrors (SESAM's) for femtosecond to nanosecond pulse generation in solid-state lasers," IEEE J. Sel. Top. Quantum Electron. **2**(3), 435–453 (1996).
18. A. Martinez and Z. Sun, "Nanotube and graphene saturable absorbers for fibre lasers," Nat. Photonics **7**(11), 842–845 (2013).
19. Y.-Z. Ma, T. Hertel, Z. Vardeny, G. Fleming, and L. Valkunas, "Ultrafast spectroscopy of carbon nanotubes," in *Carbon Nanotubes* (Springer Berlin Heidelberg, 2008), pp. 321–352.
20. D. Popa, Z. Sun, T. Hasan, W. B. Cho, F. Wang, F. Torrisi, and A. C. Ferrari, "74-fs nanotube-mode-locked fiber laser," Appl. Phys. Lett. **101**(15), 153107 (2012).
21. Z. Sun, T. Hasan, F. Wang, A. Rozhin, I. White, and A. Ferrari, "Ultrafast stretched-pulse fiber laser mode-locked by carbon nanotubes," Nano Res. **3**(6), 404–411 (2010).
22. T. Hasan, Z. Sun, F. Wang, F. Bonaccorso, P. H. Tan, A. G. Rozhin, and A. C. Ferrari, "Nanotube–polymer composites for ultrafast photonics," Adv. Mater. **21**(38â€“39), 3874–3899 (2009).
23. S. Y. Set, H. Yaguchi, Y. Tanaka, M. Jablonski, Y. Sakakibara, A. Rozhin, M. Tokumoto, H. Kataura, Y. Achiba, and K. Kikuchi, "Mode-locked fiber lasers based on a saturable absorber incorporating carbon nanotubes," in *Optical Fiber Communication Conference* (Optical Society of America, Atlanta, Georgia, 2003), p. PD44.
24. S. Y. Set, H. Yaguchi, Y. Tanaka, and M. Jablonski, "Ultrafast fiber pulsed lasers incorporating carbon nanotubes," IEEE J. Sel. Top. Quantum Electron. **10**(1), 137–146 (2004).
25. S. Y. Set, H. Yaguchi, Y. Tanaka, and M. Jablonski, "Laser mode locking using a saturable absorber incorporating carbon nanotubes," J. Lightwave Technol. **22**(1), 51–56 (2004).
26. S. Yamashita, Y. Inoue, S. Maruyama, Y. Murakami, H. Yaguchi, M. Jablonski, and S. Y. Set, "Saturable absorbers incorporating carbon nanotubes directly synthesized onto substrates and fibers and their application to mode-locked fiber lasers," Opt. Lett. **29**(14), 1581–1583 (2004).
27. T. Schibli, K. Minoshima, H. Kataura, E. Itoga, N. Minami, S. Kazaoui, K. Miyashita, M. Tokumoto, and Y. Sakakibara, "Ultrashort pulse-generation by saturable absorber mirrors based on polymer-embedded carbon nanotubes," Opt. Express **13**(20), 8025–8031 (2005).
28. S. Yamashita, Y. Inoue, K. Hsu, T. Kotake, H. Yaguchi, D. Tanaka, M. Jablonski, and S. Y. Set, "5-GHz pulsed fiber Fabry-Perot laser mode-locked using carbon nanotubes," IEEE Photon. Technol. Lett. **17**(4), 750–752 (2005).
29. V. Scardaci, Z. P. Sun, F. Wang, A. G. Rozhin, T. Hasan, F. Hennrich, I. H. White, W. I. Milne, and A. C. Ferrari, "Carbon nanotube polycarbonate composites for ultrafast Lasers," Adv. Mater. **20**(21), 4040–4043 (2008).
30. Z. Sun, A. G. Rozhin, F. Wang, V. Scardaci, W. I. Milne, I. H. White, F. Hennrich, and A. C. Ferrari, "L-band ultrafast fiber laser mode locked by carbon nanotubes," Appl. Phys. Lett. **93**(6), 061114 (2008).
31. F. Wang, A. G. Rozhin, V. Scardaci, Z. Sun, F. Hennrich, I. H. White, W. I. Milne, and A. C. Ferrari, "Wideband-tuneable, nanotube mode-locked, fibre laser," Nat. Nanotechnol. **3**(12), 738–742 (2008).
32. Z. Sun, A. G. Rozhin, F. Wang, T. Hasan, D. Popa, W. O'Neill, and A. C. Ferrari, "A compact, high power, ultrafast laser mode-locked by carbon nanotubes," Appl. Phys. Lett. **95**(25), 253102 (2009).
33. S. J. Beecher, R. R. Thomson, N. D. Psaila, Z. Sun, T. Hasan, A. G. Rozhin, A. C. Ferrari, and A. K. Kar, "320 fs pulse generation from an ultrafast laser inscribed waveguide laser mode-locked by a nanotube saturable absorber," Appl. Phys. Lett. **97**(11), 111114 (2010).
34. E. J. R. Kelleher, J. C. Travers, Z. Sun, A. C. Ferrari, K. M. Golant, S. V. Popov, and J. R. Taylor, "Bismuth fiber integrated laser mode-locked by carbon nanotubes," Laser Phys. Lett. **7**(11), 790–794 (2010).
35. C. E. S. Castellani, E. J. R. Kelleher, J. C. Travers, D. Popa, T. Hasan, Z. Sun, E. Flahaut, A. C. Ferrari, S. V. Popov, and J. R. Taylor, "Ultrafast Raman laser mode-locked by nanotubes," Opt. Lett. **36**(20), 3996–3998 (2011).
36. R. Going, D. Popa, F. Torrisi, Z. Sun, T. Hasan, F. Wang, and A. C. Ferrari, "500 fs wideband tunable fiber laser mode-locked by nanotubes," Physica E **44**(6), 1078–1081 (2012).
37. J. S. Lauret, C. Voisin, G. Cassabois, C. Delalande, P. Roussignol, O. Jost, and L. Capes, "Ultrafast carrier dynamics in single-wall carbon nanotubes," Phys. Rev. Lett. **90**(5), 057404 (2003).
38. Y.-C. Chen, N. R. Raravikar, L. S. Schadler, P. M. Ajayan, Y.-P. Zhao, T.-M. Lu, G.-C. Wang, and X.-C. Zhang, "Ultrafast optical switching properties of single-wall carbon nanotube polymer composites at 1.55 μm," Appl. Phys. Lett. **81**(6), 975–977 (2002).
39. Z. Zhang, L. Wang, and Y. Wang, "Sub-100 fs and passive harmonic mode-locking of dispersion-managed dissipative fiber laser with carbon nanotubes," J. Lightwave Technol. **31**(23), 3719–3725 (2013).
40. Z. Yu, Y. Wang, X. Zhang, X. Dong, J. Tian, and Y. Song, "A 66 fs highly stable single wall carbon nanotube mode locked fiber laser," Laser Phys. **24**(1), 015105 (2014).
41. Z. Sun, T. Hasan, and A. C. Ferrari, "Ultrafast lasers mode-locked by nanotubes and graphene," Physica E **44**(6), 1082–1091 (2012).

#231628 - $15.00 USD Received 30 Dec 2014; revised 31 Mar 2015; accepted 3 Apr 2015; published 10 Apr 2015

42. Z. Sun, T. Hasan, F. Torrisi, D. Popa, G. Privitera, F. Wang, F. Bonaccorso, D. M. Basko, and A. C. Ferrari, "Graphene mode-locked ultrafast laser," ACS Nano **4**(2), 803–810 (2010).
43. Z. Luo, M. Zhou, J. Weng, G. Huang, H. Xu, C. Ye, and Z. Cai, "Graphene-based passively Q-switched dual-wavelength erbium-doped fiber laser," Opt. Lett. **35**(21), 3709–3711 (2010).
44. H. Zhang, S. B. Lu, J. Zheng, J. Du, S. C. Wen, D. Y. Tang, and K. P. Loh, "Molybdenum disulfide (MoS_2) as a broadband saturable absorber for ultra-fast photonics," Opt. Express **22**(6), 7249–7260 (2014).
45. R. I. Woodward, E. J. R. Kelleher, R. C. T. Howe, G. Hu, F. Torrisi, T. Hasan, S. V. Popov, and J. R. Taylor, "Tunable Q-switched fiber laser based on saturable edge-state absorption in few-layer molybdenum disulfide (MoS_2)," Opt. Express **22**(25), 31113–31122 (2014).
46. M. Zhang, R. I. Woodward, E. J. R. Kelleher, F. Torrisi, G. Hu, S. V. Popov, J. R. Taylor, and T. Hasan, "MoS2-PVA composite for sub-bandgap mode-locking of a wideband tunable ultrafast Er:fiber laser," Nano Res. 10.1007/s12274-014-0637-2 (2014).
47. Y. Huang, Z. Luo, Y. Li, M. Zhong, B. Xu, K. Che, H. Xu, Z. Cai, J. Peng, and J. Weng, "Widely-tunable, passively Q-switched erbium-doped fiber laser with few-layer MoS2 saturable absorber," Opt. Express **22**(21), 25258–25266 (2014).
48. T. Schreiber, B. Ortaç, J. Limpert, and A. Tünnermann, "On the study of pulse evolution in ultra-short pulse mode-locked fiber lasers by numerical simulations," Opt. Express **15**(13), 8252–8262 (2007).
49. G. Agrawal, *Nonlinear Fiber Optics* (Academic Press, 2012).
50. O. Okhotnikov, A. Grudinin, and M. Pessa, "Ultra-fast fibre laser systems based on SESAM technology: new horizons and applications," New J. Phys. **6**, 177 (2004).
51. K. Tamura, L. E. Nelson, H. A. Haus, and E. P. Ippen, "Soliton versus nonsoliton operation of fiber ring lasers," Appl. Phys. Lett. **64**(2), 149–151 (1994).
52. D. von der Linde, "Characterization of the noise in continuously operating mode-locked lasers," Appl. Phys. B **39**(4), 201–217 (1986).
53. V. J. Wittwer, C. A. Zaugg, W. P. Pallmann, A. E. H. Oehler, B. Rudin, M. Hoffmann, M. Golling, Y. Barbarin, T. Sudmeyer, and U. Keller, "Timing jitter characterization of a free-running SESAM mode-locked VECSEL," IEEE Photon. J. **3**(4), 658–664 (2011).

1. Introduction

Passively mode-locked ultrafast pulses, in particular, with <100 fs duration, have found important scientific applications such as ultrafast laser spectroscopy [1], supercontinuum generation [2] and optical metrology [3]. Mode-locked solid state lasers are the conventional technology to generate these kind of pulses due to the low dispersion and nonlinearity of the gain medium [4]. However, they are complex, expensive and prone to misalignment compared to fiber lasers with simple and compact designs, efficient heat dissipation and alignment-free operation [5]. Although mode-locked fiber lasers normally have large nonlinear effects and high-order dispersion which limit the accessible pulse duration to several hundred femtoseconds, appropriate interplay between dispersion, nonlinearity, saturable absorber (SA) and gain medium still provides the possibility of generating sub-100 fs pulses [5–7].

In compact ultrafast fiber lasers, cavity chromatic dispersion control is always a key factor. On one hand, the interaction of anomalous dispersion with fiber nonlinearity can result in soliton-like mode-locking. In this regime, solitons result from the cancellation of phase perturbations due to the negative dispersion and self-phase modulation (SPM) [5]. The pulse width is determined by the cavity dispersion, $\tau \propto \sqrt{|\beta_2| \times L}$, where β_2 [s^2/m] is the average group velocity dispersion (GVD) parameter and L [m] is the cavity length [7]. On the other hand, combination of normal cavity dispersion, nonlinearity, gain medium and SA can result in different mode-locking regimes, known as self-similar regime with dispersion maps (consisting of segments of normal and anomalous GVD) or dissipative solitons (DSs) without dispersion maps [8]. Both self-similar regime and DSs have higher free-wave-breaking pulse energy than that of solitons. Also, their output pulses have large normal chirp, which can be dechirped by using an external compressor [8]. Regardless of mode-locking regimes, the output dechirped pulse width in an ultrafast laser is strongly influenced by the cavity dispersion and reaches to a minimum when the net cavity dispersion approaches zero [8,9]. It should be noted that 'zero net dispersion' does not mean the use of zero GVD fiber. Without the effects of GVD, the mode-locking will become unstable. The appropriate way to construct a cavity with net dispersion close to zero is to employ dispersion maps that alternate segments of large anomalous and normal dispersion fibers. This leads to periodic broadening and

#231628 - $15.00 USD Received 30 Dec 2014; revised 31 Mar 2015; accepted 3 Apr 2015; published 10 Apr 2015

compression of the intra-cavity pulses, such that the pulse maintains its minimum duration only over small segments of the cavity, reducing the nonlinear optical effects. This configuration is known as stretched-pulse design [7,10]. Tamura first proposed this configuration and obtained 77-fs pulses in a fiber laser [10]. It is now theoretically and experimentally established that this design can support shorter pulses than other regimes in mode-locked fiber lasers [11–14]. Also, it is of great practical importance to study the laser cavity pulse dynamics when the cavity GVD is close to zero. This cannot only reveal the comprehensive pulse formation dynamics (*e.g.*, transition between different mode-locking regimes from soliton-like mode-locking, stretched-pulse mode-locking to similarition or DSs mode-locking regime), but also can potentially lead to high energy and short pulse duration ultrafast lasers.

To design an ultrafast laser, in addition to the cavity design, the recovery time and modulation depth of the SA are two important factors to consider [13,15]. As demonstrated in [16], a SA with fast response time is less affected by amplified spontaneous emission (ASE) and consequently exhibits better self-starting capability compared to slow SAs in presence of high-power ASE. The modulation depth is defined as the maximum change of absorption in SA under different light intensity. According to the Fourier transform theory, the shorter the dechirped pulse, the wider the bandwidth, leading to lower gain for these pulses due to gain spectral filtering. A higher modulation depth is required to compensate the extra loss of shorter pulses caused by the lower gain compared with wider dechirped pulses, especially for fiber lasers which experience large loss per round trip [13]. Thus, a high modulation depth helps achieving a short pulse duration [17]. Therefore, employing a fast SA with high modulation depth is advantageous to get ultrafast pulses [13]. Single-wall carbon nanotubes (SWNTs) have been widely demonstrated as a good SA material [18] due to their sub-picosecond recovery time [19], high modulation depth (more than 17% in [20] when suitable nanotubes and diameter distributions are used with respect to operating wavelength), wide (*e.g.* >300 nm [21]) operation bandwidth (depending on diameter distributions) and ease of device fabrication through solution processing [22]. SWNT-SAs are particularly advantageous for fiber lasers [23–36] as they can be easily integrated into the cavity while preserving an alignment-free all-fiber configuration. In addition, the recovery time of SWNTs contains a fast time constant (in the order of 100 fs) and a slow one (1~15 ps) [37,38] associated with the intraband carrier thermalization and interband carrier recombination [19], respectively. The slow recovery facilitates self-starting mode-locking while the fast recovery helps to shape and shorten pulses [14]. Taking the advantages of the SWNT-SA properties, sub-100 fs pulses from fiber lasers have already been successfully achieved [20,39]. Indeed, the shortest pulse directly from SWNT mode-locked fiber lasers reported is 66 fs [40], which is based on the stretched-pulse design.

To date, mode-locked fiber lasers operating at around zero cavity GVD based on diverse SAs including SWNTs have been widely investigated in experiments [10,11,13,14,20,40]. They all work in stretched-pulse mode-locking regime. Pulse dynamics in stretched-pulse regime has also been experimentally studied [11]. However, there is no systematic report linking experimental pulse dynamics with numerical modelling near zero cavity GVD. In particular, the transition between different mode-locking regimes has not yet been fully investigated through experiments or numerical simulations. In this paper, we develop a numerical model to study different mode-locking regimes near zero cavity GVD and the transition between them for the first time. We also verify the model via experiments. An SWNT-based transmission-type SA is chosen both in the simulations and experiments which therefore can make our numerical model efficiently apply to other SAs based on new nanomaterials (such as graphene [18,41–43] and MoS_2 [44–47]). In addition, comparing to traditionally artificial SAs (*e.g.* nonlinear polarization rotation) which it is difficult to experimentally quantify and reproduce the achieved modulation depth and saturation power, the saturable absorption parameters of SWNT-SA can be experimentally measurable and reproducible, thus making our model high reliability. Finally, we experimentally achieve ~97 fs pulses in stretched-pulse regime by using this SA. The corresponding experimental results

#231628 - $15.00 USD Received 30 Dec 2014; revised 31 Mar 2015; accepted 3 Apr 2015; published 10 Apr 2015

are in good agreement with the numerical simulations. Other mode-locking regimes are also experimentally realized and exhibit the same trends with numerical simulations.

2. Numerical simulations

2.1 Model

The numerical model is based on an experimental erbium-doped fiber (EDF) ring laser; see Fig. 1(a). This laser cavity consists of EDF, polarization independent optical isolator (ISO), output coupler (OC), 980/1550 nm wavelength division multiplexer (WDM), in-line polarization controller (PC) and SA. The EDF is pumped by a 974 nm laser diode (LD). The in-line PC is chosen not only to optimize mode-locking operation, but to also make the cavity short. Another ISO is connected to the output port to remove the residual pump power. The SA is placed after the ISO where the intra-cavity power is the lowest, minimizing any possible thermal damage to the SA. In the ring cavity, the OC, ISO and PC are all made by single mode fiber (SMF, Corning SMF-28), marked as SMF 1, SMF 2 and SMF 3, respectively. Thus, this cavity is equivalent to the inset of Fig. 1(a) in our model. All of the parameters (corresponding to ~1.5 μm operation wavelength) in this cavity are listed in Table 1, which are obtained from their experimental values .

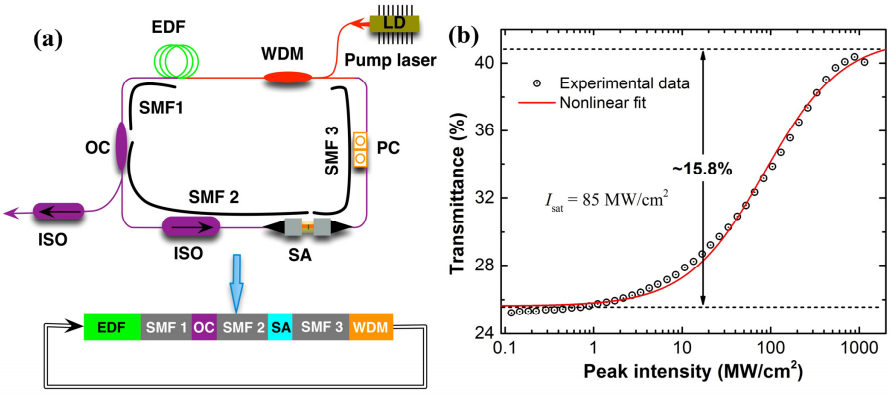

Fig. 1. (a) Experimental fiber laser configuration for the numerical simulations. (b) Nonlinear transmittance of SWNT-SA as a function of input pulse peak intensity.

Table 1. Parameters of the numerical simulations

EDF	OC	SMF	WDM fiber	SWNT-SA
β_2 = 38 ps^2/km g_0 = 30 dB $P_{sat,G}$ = 1.4 mW $\Delta\omega$ = 40 nm γ = 5.3 m^{-1}kW^{-1} L_{EDF} = 1.35 m	20% output (*i.e.* T = 80%)	β_2 = –22 ps^2/km γ = 1.1 m^{-1}kW^{-1} L_{SMF1} = 0.3 m L_{SMF2} = 0.95 m L_{SMF3} is variable (0.1 to ~2 m)	β_2 = –7 ps^2/km γ = 2.1 m^{-1}kW^{-1} L_{WDM} = 0.25 m	T_0 = 25% ΔT = 15.8% $P_{sat,A}$ = 72 W

In our simulation, each part of the cavity is separately simulated [48]. Both the passive and active fibers are modeled by the nonlinear Schrödinger Equation (NLSE) [49] with gain (g)

$$\frac{\partial A}{\partial z} = -i\frac{\beta_2}{2}\frac{\partial^2 A}{\partial \tau^2} + i\gamma|A|^2 A + \frac{g}{2}A \qquad (1)$$

where, $A(\tau, z)$ is the electric field envelope, z is the propagation position along the fiber axis, τ is the pulse local time, and γ represents the fiber nonlinearity. In passive fiber, the gain is zero. Here, we assume the loss of passive fiber is zero as the overall loss is very small (<5 × 10^{-5} dB). High-order cavity dispersion and other nonlinearity effects (*e.g.*, Raman scattering

#231628 - $15.00 USD Received 30 Dec 2014; revised 31 Mar 2015; accepted 3 Apr 2015; published 10 Apr 2015

effect), negligible in our experiment, are not considered in the simulation. For an active fiber, g denotes the saturation gain, which has a spectral dependence $g(\omega)$. The effect of gain spectral dependence is evaluated in the frequency domain using a Lorentzian line shape, with a typical 40 nm bandwidth and 1554 nm central wavelength. This numerical model is solved with standard split-step Fourier method [49]. It is worth noting that the gain-cross section is very small for ordinary rare-earth doped fiber lasers, such that the gain saturation due to a single pulse energy is negligible [15]. In this case, the gain saturates only over many pulses, *i.e.* with the average power. The gain saturation is therefore given by

$$g(P_{\text{ave}}) = \frac{g_0}{1 + P_{\text{ave}} / P_{\text{sat,G}}} \tag{2}$$

where, g_0 is the small-signal gain and $P_{\text{sat,G}}$ is the saturation power of gain medium, $P_{\text{ave}} = E_{\text{p}} / T_{\text{R}}$ is the average power with T_{R} as the cavity round trip time and E_{p} as the single pulse energy.

The SA used in our model is based on SWNT, which is produced by laser ablation technique and is sonicated with sodium-carboxymethylcellulose (Na-CMC) in water (as the dispersant and host polymer) and centrifuged. Slow evaporation of water forms free-standing SWNT-SA with individualized SWNTs. Detailed fabrication method is described in [22]. The SA is modeled by a transfer function that describes its transmittance [48]

$$T = T_0 + \Delta T \cdot (1 - \frac{1}{1 + P / P_{\text{sat,A}}}) \tag{3}$$

where, T_0 is linear transmission at low incident power, ΔT is saturable loss (*i.e.* modulation depth), P is the instantaneous pulse peak power and $P_{\text{sat,A}}$ is the saturation power of the SA. The parameters of this SWNT-SA is measured with an optical parametric oscillator. This oscillator can deliver sub-200 fs pulses with 80 MHz repetition rate at ~1550 nm. Light from the oscillator is then coupled into SMF-28 to measure the SWNT-SA sandwiched between two fiber connectors. The pulse duration at the position of SWNT-SA is ~300 fs after stretching due to fiber dispersion. By varying the oscillator power, we obtain power-dependent transmittance measurement of SWNT-SA; see Fig. 1(b). The linear transmittance (*i.e.*, transmittance at low power) is ~25%. The data is fitted using Eq. (3), giving ~15.8% modulation depth and ~72 W saturation power (assuming a 10.4 μm fiber core); see Table 1.

2.2 Simulation results

In our model, the active (EDF) and passive (SMF) fiber present different signs of dispersion. Thus, the simplest way to vary the net cavity dispersion can be realized by tailoring the length of the SMF. We choose L_{SMF3} ranging from 0.1 to ~2 m with 0.03 m step, giving the variation of total cavity length ($L_{\text{cavity}} = L_{\text{EDF}} + L_{\text{SMF1}} + L_{\text{SMF2}}$) and net cavity dispersion from 2.95 to 4.87 m and 0.02 to –0.023 ps^2 (with 660 fs^2 step), respectively. We assume the stable solutions are reached as soon as the relative pulse energy change ($|\Delta E_p|/E_p$) in two consecutive round trips is smaller than 10^{-8}. Self-starting mode-locking is readily reached with a 1 ps Gaussian pulse as the initial field. The same stable pulse profile can also be realized from white noise field in this model, only with random pulse-local-time due to the noise characteristics. Figure 2 shows the simulated output spectra and pulse intensity directly from 20% port of OC. The spectral bandwidth reaches its maximum (32.4 nm) when the net cavity dispersion is slightly positive ($\beta_{\text{net}}^{(2)}$ = 0.002 ps^2, L_{cavity} = 3.73 m), and decreases to 16.7 and 15.1 nm along the two sides of 0.002 ps^2. The output pulse width changes slowly at the anomalous dispersion side, and then significantly increases along with dispersion at the normal dispersion side; see Fig. 2(b) and inset of Fig. 2(b). Another visible feature of Fig. 2(a) is that the spectra has a parabolic shape (in dB scale) as soon as $\beta_{\text{net}}^{(2)}$>0.005 ps^2, a typical output feature of self-similar regime [6].

#231628 - $15.00 USD Received 30 Dec 2014; revised 31 Mar 2015; accepted 3 Apr 2015; published 10 Apr 2015

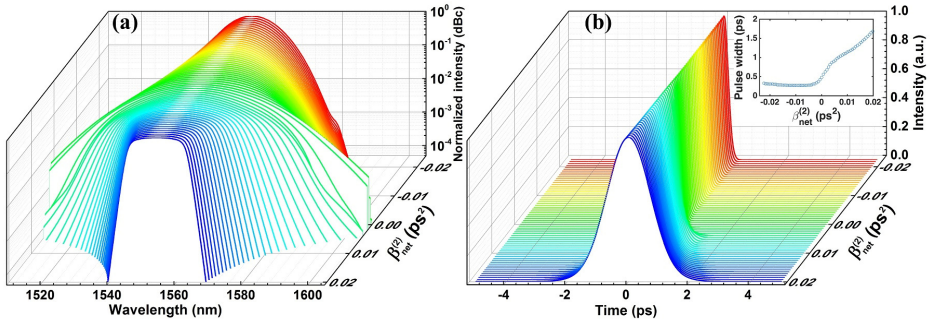

Fig. 2. Output (a) spectra and (b) pulse with different net cavity dispersion. Inset: Pulse width against net cavity dispersion.

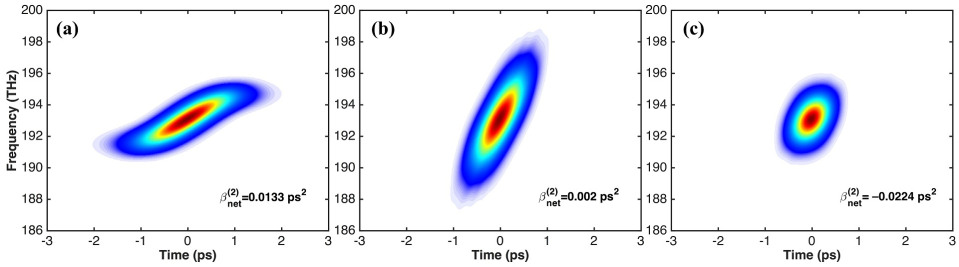

Fig. 3. Spectrograms of output pulse for three $\beta^{(2)}_{net}$ (a) 0.0133, (b) 0.002, (c) –0.0224 ps^2. (linear scale: 0 max)

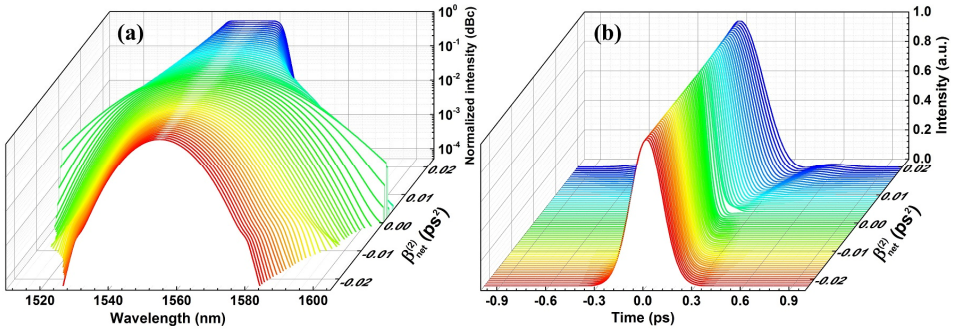

Fig. 4. (a) Output spectrum and (b) pulse intensity after compression with different net cavity dispersion.

To obtain the chirp information of the output pulse from OC, the spectrograms of pulses for three representative dispersions: 0.0133, 0.002 and –0.0224 ps^2 are presented in Fig. 3, all exhibiting positive chirp [48]. For Figs. 3(b) and 3(c), the pulses are almost linearly positively chirped and hence can be dechirped to transform-limited pulses. Such pulses are important for various applications such as chirped pulse amplification (CPA) [5]. In Fig. 3(a), although the two wings of the pulses are nonlinearly chirped, the linear chirp is still dominant and compression of the pulses close to transform-limited value is possible [10]. The dechirped spectra and pulse intensity are shown in Fig. 4. Here, in order to clearly observe the output features both at anomalous and normal dispersion region, the simulation results at the anomalous dispersion side are placed at the front. The dechirped spectral characteristics are almost similar to those observed in Fig. 2(a). However, the dechirped pulses change significantly compared to that in Fig. 2(b). The dechirped pulse duration reaches to a

#231628 - $15.00 USD Received 30 Dec 2014; revised 31 Mar 2015; accepted 3 Apr 2015; published 10 Apr 2015

minimum of 102.5 fs at $\beta_{net}^{(2)}$ = 0.002 ps^2 and then increases along the two sides of this dispersion value. Thus, as discussed above, the maximum spectral bandwidth (32.4 nm) and minimum pulse duration (102.5 fs) can be obtained at slightly positive dispersion, as predicted in [50,51].

Thus far, we have systematically analyzed the output spectra and pulses. To get further insights into the mode-locking regime of these pulses, we next investigate the intra-cavity pulse dynamics. Figure 5(a) depicts the intra-cavity pulse evolution with net cavity dispersion ranging from 0.02 to –0.023 ps^2, *i.e.* from shortest (deep blue line) to longest cavity (deep red line). On one hand, for $\beta_{net}^{(2)}$ = 0.004 to –0.023 ps^2, the pulses compress and stretch twice per cavity round-trip, and reach a minimum (and nearly transform-limited) in each segment. This is known as stretched-pulse mode-locking [6]. On the other hand, for $\beta_{net}^{(2)}$ = 0.004 to 0.02 ps^2, the pulses compress and stretch only once, with a minimum duration (with large normal chirp) at the beginning of the normal dispersion fiber. This is the typical feature of self-similar regime [6]. Note that the SPM is no longer balanced by GVD at large normal dispersion [6,8]. Other mechanisms, such as gain spectral filtering and saturable absorption, are needed to induce to self-start and maintain mode-locking. Apparently, the SWNT-SA plays an important role to shorten the pulse, because the pulse duration decreases abruptly after SWNT-SA (see the dotted box in Fig. 5(a)). In summary, the transition from stretched-pulse regime to self-similar regime in this model occurs at a ~0.004 ps^2.

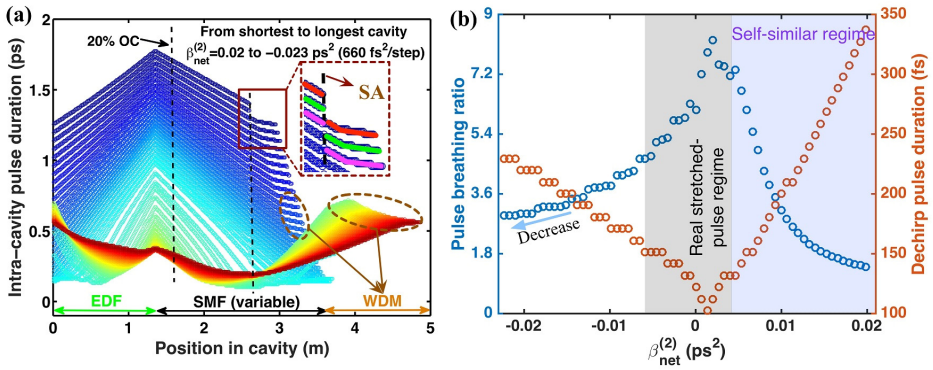

Fig. 5. (a) Intra-cavity pulse evolution with different net cavity dispersion. (b) Dechirped pulse duration and intra-cavity pulse breathing ratio as a function of net cavity dispersion.

The remaining question is what the net cavity dispersion is when the stretched-pulse regime evolves into the soliton-like regime. Figure 5 shows that the pulse evolution becomes smoother (see Fig. 5(a)) and intra-cavity pulse breathing ratio (*i.e.* the ratio of maximal to minimal pulse duration) becomes smaller (see Fig. 5(b)) at larger negative dispersion. With further simulations, we obtain the boundary value between stretched-pulse and soliton-like regime to be ~-0.03 ps^2, where the stretched-pulse feature (twice compression and stretching) disappears and pulse breathing ratio decreases to 2.2, a fourth of the maximum. Thus, for $\left|\beta_{net}^{(2)}\right|$>0.03 ps^2 at anomalous dispersion region, the laser should work in usual soliton-like regime [51]. However, the original purpose of stretched-pulse design is to support high energy and shortest pulse possible (after compression) [10,12]. To achieve this, the intra-cavity pulse breathing ratio should be large enough (*e.g.* >10) [6,7,51]. Thus the average intra-cavity pulse duration is large which in turn reduces the nonlinearity to support high energy (and short duration) [10]. Hence, we define an area in stretched-pulse regime with net cavity dispersion ranging from ~–0.006 to 0.004 ps^2 (L_{cavity} = 3.76~4.12 m), depicted as the gray area in Fig. 5(b). In this area, the pulse duration is <1.5 times of the shortest duration (102.5 fs) and also the breathing ratio is higher than two third of maximum (8.3). Since it is possible to

#231628 - $15.00 USD Received 30 Dec 2014; revised 31 Mar 2015; accepted 3 Apr 2015; published 10 Apr 2015

achieve shortest pulse duration and a large breathing ratio in this area, we regard it as the real stretched-pulse regime instead of the area defined by $\beta_{net}^{(2)} = -0.03$ to 0.004 ps^2. In other words, to achieve ultra-short pulses, a designer could make fiber lasers work in this area. Note that the cavity length with zero net dispersion (L_0) is ~3.8 m in this model. Different L_0 will result in different dispersion range for the real stretched-pulse regime. However, detailed study in this is out of the scope of this work.

3. Experimental results and discussions

Based on the numerical simulation results, we build an experimental laser setup (see Fig. 1(a)) with all parameters listed in Table 1. In our experimental setup, we first set L_{SMF3} as 1 m, leading to 3.85 m cavity length. The total intra-cavity dispersion is ~50 fs^2 (~0 ps^2, located within the gray area in Fig. 5(b)), typical for stretched-pulse fiber lasers. Continuous wave starts at ~27 mW pump power. Self-starting mode-locking is observed at 79.5 mW pump power. At 116 mW pump power, we obtain 3.93 mW output power with 73.1 pJ pulse energy. The repetition rate is 53.78 MHz, corresponding to 18.5 ns cavity round-trip time. Figure 6(a) shows the output spectrum without soliton sideband signatures. The central wavelength and FWHM bandwidth are 1554 nm and 41.44 nm, respectively. We use SMF-28 fiber to compress the pulse duration due to the large linearly positive chirp of pulses from stretched-pulse cavity [10]. The optimal length is ~0.5 m. The autocorrelation trace is shown in Fig. 6(b). A Gaussian profile fits quite well with experimental results, as expected for stretched-pulse fiber lasers [5,10]. The FWHM is 138 fs. Deconvolution gives ~97.5 fs duration. The time-bandwidth product (TBP) is 0.49 (1.11 times the transform-limit of a Gaussian pulse), indicating slightly chirped output pulses. Further, to investigate the noise characteristics and stability of pulses, we use von der Linde method to measure the timing jitter (1.24 ps) and pulse amplitude fluctuation (0.0028%) [52,53]. These results indicate that our stretched-pulse cavity can generate high quality pulses.

Since the stretched-pulse mode-locking was already realized in experiments, we use the numerical model developed in *Section 2* to simulate the cavity and verify its reliability. All of the simulation parameters are taken from their experimental values. We set the saturation power of the gain fiber to 3.6 mW to make simulation pulse energy comparable to that obtained in the experiment. Other parameters of EDF and SMFs can be found in Table 1. Using these parameters, self-starting mode-locking operation is obtained. The output pulse energy is 70.4 pJ (close to the experimental value 73.1 pJ). The optimal length of SMF-28 for dechirp is 0.5 m, matching experimental value. The dechirped spectrum and pulse are illustrated in Fig. 6(a) and the inset of Fig. 6(b), respectively. Experimental spectrum matches well with simulation results. The simulation pulse duration is ~102 fs, similar to the experimental value 97.5 fs. Note that the experimental pulse is measured using an autocorrelator. It is therefore a convolution structure, making it impossible to directly compare between experimental and simulation results; see Fig. 6(b). Figure 6(c) gives the intra-cavity pulse duration and bandwidth evolution along the cavity position. The pulse is compressed and stretched twice per cavity round trip, as expected for stretched-pulse design [6,10]. The pulse breathing ratio reaches 13.2. This implies that the net cavity dispersion is likely to be located within the gray area in Fig. 5(b). The net dispersion value 50 fs^2 (~0 ps^2) confirms the prediction. Also, Fig. 6(c) shows the gain spectral filtering and SWNT-SA play an important role on pulse spectrum narrowing, which help sustaining of ultrafast pulses [6]. Note that $P_{sat,G}$ parameters (*i.e.*, pump powers) are different between the simulations shown in Figs. 6(c) and 5(a). $P_{sat,G} = 3.6$ mW is obtained from our experiments used in Fig. 6(c). This choice is based on the fact that the generated pulse energy fits well with experimental results of our stretched-pulse cavity. On the other hand, $P_{sat,G} = 1.4$ mW (see Table 1) in Fig. 5(a) is used to simulate the pulse dynamics from ~–0.02 to 0.02 ps^2 and avoid pulse breaking or reaching distortion threshold (*e.g.*, $P_{sat,G}>3$ mW can lead to pulse breaking or distortion in the soliton-like regime from our simulations) for all three mode-locking regimes Thus, the intra-cavity pulse durations do not overlap between Figs. 6(c) and 5(a). In summary, the

#231628 - $15.00 USD Received 30 Dec 2014; revised 31 Mar 2015; accepted 3 Apr 2015; published 10 Apr 2015

experimental results in this stretched-pulse cavity are well agreements with our simulation results, indicating high reliability of proposed model.

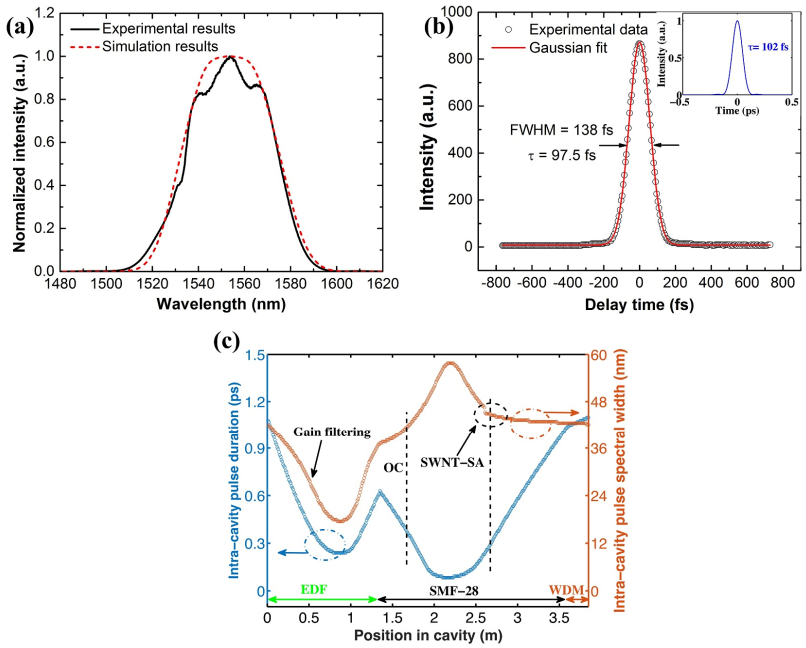

Fig. 6. Mode-locking results. (a) Output spectrum. (b) Autocorrelation trace of pulse, with Gaussian fit. Inset: Output pulse from simulations. (c) Intra-cavity pulse duration and spectral width at different cavity position of this stretched-pulse cavity.

To investigate other mode-locking regimes in experiments, we vary the net cavity dispersion by tailoring the length of the SMF (see Fig. 1(a)). Three sets of $\beta_{net}^{(2)}$ are chosen as 0.0082, –0.0117 and –0.0233 ps^2, corresponding to 3.48, 4.38 and 4.91 m of cavity length, respectively. Note that in our experiments, it is not easy to get normal dispersion >0.02 ps^2 (requiring ultra-short cavity) due to the limited length of optical components (*e.g.* OC, ISO, PC). Thus, we replace the EDF of stretched-pulse cavity by a new EDF with β_2 = 58 ps^2/km and 1.3 m length. This gives $\beta_{net}^{(2)}$ = 0.024 ps^2. Thus, including the stretched-pulse cavity, we have five cavities with $\beta_{net}^{(2)}$ = 0.024, 0.0082, ~0 (50 fs^2), –0.0117 and –0.0233 ps^2, all of which can stably self-start mode-locking. The related output spectra (Fig. 7(a)) and autocorrelation traces (Fig. 7(b)) of dechirped pulse are recorded when the output pulse energy is maximum. Notably, the spikes in the spectra result from the continuous wave component in cavity rather than Kelly sidebands. The experimental spectra and pulses show the same trends with simulations (see Fig. 4). Shortest pulses and widest bandwidth can be achieved at a slightly positively dispersion (50 fs^2, close to zero). As discussed in Section 2.2, the front two sets of spectra in Fig. 7(a) work on self-similar regime with pulse energy of 78 pJ and 79.2 pJ, respectively while the other three sets of cavity are expected to work in the stretched-pulse regime. However, for $\beta_{net}^{(2)}$ = –0.0117 ps^2 and –0.0233 ps^2, the output pulses show some soliton-like features. As shown in Figs. 7(c) and 7(d), the output spectrum and autocorrelation trace can be better fitted by sech^2 shape than Gaussian shape for $\beta_{net}^{(2)}$ = –0.0117 ps^2, giving the evidence of soliton-like features. Table 2 summarizes the output parameters for these five sets of dispersion. The last two sets are better fitted by sech^2 shape than Gaussian. Hence, as soon as $\left|\beta_{net}^{(2)}\right|$ ≥0.012 ps^2 in anomalous dispersion region, mode-locking no longer remains in the typical stretched-pulse regime, but evolves into soliton-like regime without sideband features.

#231628 - $15.00 USD Received 30 Dec 2014; revised 31 Mar 2015; accepted 3 Apr 2015; published 10 Apr 2015

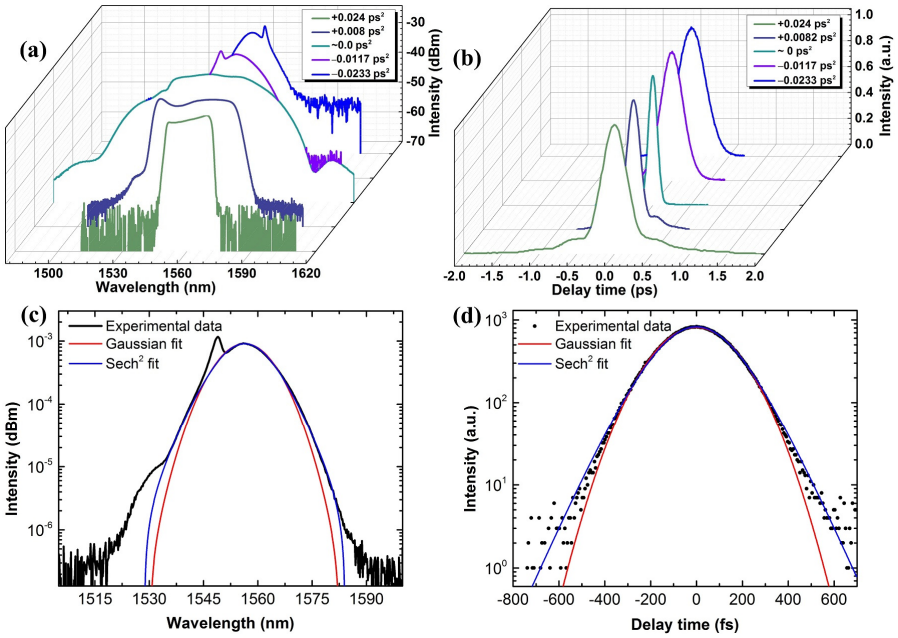

Fig. 7. (a) Output spectrum, and (b) autocorrelation trace of dechirped pulse with different cavity dispersion. (c) Output spectrum, and (d) autocorrelation trace of dechirped pulse with Gaussian and sech^2 fit at –0.0117 ps^2.

Table 2. Laser output parameters for different net dispersion value

Net dispersion (ps^2)	0.024	0.0082	~0	–0.0117	–0.0233
Pulse width (fs)	294.7	146	97.5	213	265
Spectral width (nm)	22	38	41.44	15.6	10.8
TBP	0.805	0.69	0.49	0.411	0.355
Pulse energy (pJ)	79.2	78	73.1	60	49.6

4. Conclusion

We present our study and analysis of pulse dynamics of SWNT-SA mode-locked fiber lasers near zero cavity GVD using a numerical model based on NLSE. We show that the shortest pulses can be obtained at a slightly positive cavity dispersion in the stretched-pulse regime. We also investigate the transition from stretched-pulse regime to other mode-locking regimes. From our numerical simulations, the net cavity dispersion for the transition from stretched-pulse to self-similar regime is ~0.004 ps^2. The transition to soliton-like regime occurs at ~-0.03 ps^2. However, the experimental results demonstrate that as soon as $\left|\beta_{net}^{(2)}\right| \geq 0.012$ ps^2 in anomalous dispersion region, the mode-locking state no longer remains in typical stretched-pulse regime but evolves into a soliton-like regime. We define an area with net cavity dispersion ranging from –0.006 to 0.004 ps^2 (L_{cavity} = 3.76~4.12 m), which could be regarded as real stretched-pulse regime allowing shortest pulses. With the assistance of the numerical model, we experimentally design a stretched-pulse cavity with $\beta_{net}^{(2)}$ = 50 fs^2 (~0 ps^2) and achieve pulses with ~97 fs duration and ~41 nm bandwidth. The experimental results are in good agreement with the simulations. The different mode-locking regimes that we obtain in experiments exhibit the same trends with simulations, confirming the reliability of our model. Our analysis can aid researchers efficiently designing different mode-locking regimes based

#231628 - $15.00 USD Received 30 Dec 2014; revised 31 Mar 2015; accepted 3 Apr 2015; published 10 Apr 2015

on other new SA nanomaterials (such as graphene [18,41,42] and MoS_2 [44–46]) and achieving ultra-short pulse duration.

Acknowledgments

We thank Dr. Valentin Wittwer for useful discussions on noise characterization. We acknowledge funding from the National Natural Science Foundation of China (Grant No. 61275050, 61275144), Teknologiateollisuus TT-100, the European Union's Seventh Framework Programme (REA grant agreement No. 631610), and Aalto University (Finland). TH acknowledges funding from the Royal Academy of Engineering through a research fellowship (Graphlex).

#231628 - $15.00 USD Received 30 Dec 2014; revised 31 Mar 2015; accepted 3 Apr 2015; published 10 Apr 2015